Bistatic Sonobuoy Deployment Strategies for Detecting Stationary and Mobile Underwater Targets

Mumtaz Karatas
(1) Industrial Engineering Department
Naval Academy, National Defense University
Istanbul, 34940, TURKEY
mkaratas@dho.edu.tr

(2) Bahcesehir University
Istanbul, 34353, TURKEY

Emily Craparo
Department of Operations Research
Naval Postgraduate School
Monterey, CA 93943, USA
emcrapar@nps.edu

Gülşen Akman
Industrial Engineering Department
Kocaeli University
Kocaeli, 41380, TURKEY
akmang@kocaeli.edu.tr

ABSTRACT

The problem of determining effective allocation schemes of underwater sensors for surveillance, search, detection, and tracking purposes is a fundamental research area in military OR. Among the various sensor types, multistatic sonobuoy systems are a promising development in submerged target detection systems. These systems consist of sources (active sensors) and receivers (passive sensors), which need not be collocated.

A multistatic sonobuoy system consisting of a single source and receiver is called a bistatic system. The sensing zone of this fundamental system is defined by Cassini ovals. The unique properties and unusual geometrical profile of these ovals distinguish the bistatic sensor allocation problem from conventional sonar placement problems. This study is aimed at supporting decision makers in making the best use of bistatic sonobuoys to detect stationary and mobile targets transiting through an area of interest. We use integral geometry and geometric probability concepts to derive analytic expressions for the optimal source and receiver separation distances to maximize the detection probability of a submerged target. We corroborate our analytic results using Monte Carlo simulation. Our approach constitutes a valuable "back of the envelope" method for the important and difficult problem of analyzing bistatic sonar performance.

Keywords: Bistatic Sonar, Multistatic Sonar, Moving Target, Detection, Monte Carlo Simulation, Anti-Submarine Warfare.

1. INTRODUCTION

The concept of countering submerged targets using multistatic sonobuoy systems in anti-submarine warfare (ASW) is of increasing interest. A multistatic sonobuoy network consists of sources and receivers which operate by emitting sound energy from a source into the water and listen for the reflected echoes returning across the receivers to detect targets. The source of energy can be an ASW ship with a hull-mounted sonar device, a helicopter equipped to dip a sonar device, or an active sonobuoy dropped by a

maritime patrol aircraft. A sonobuoy is defined as an immobile, expendable sonar device that is dropped or ejected from an aircraft or ship for ASW or underwater acoustic research purposes. The receiver can be a passive sonar device attached to a ship, a passive sonobuoy, or a stationary hydrophone system (Washburn, 2010).

In a monostatic system the source and receiver are collocated, whereas in a multistatic system they may be separated by some distance. Each source-receiver pair in a multistatic system forms a bistatic system. In this paper, a "bistatic sonobuoy couple" describes a single source (active sonobuoy) and receiver (passive sonobuoy).

Multistatic systems have several advantages over monostatic systems. One such advantage is covertness due to the passive nature of the receivers. As stated by Cox (1989), "countermeasure tactics are greatly complicated if the target does not know the position of the receivers." In addition, multistatic systems enable multi-angle observations and therefore improve tracking accuracy. In their studies, Coon (1997) and Simakov (2008) consider merging data from multiple detections into a single alert and reducing false alarms to enable more precise localization in multistatic sonar networks. Multistatic sonar networks also allow multi-platform operations such as an airplane that deploys passive sonobuoys while a surface ship or a dipping helicopter deploys active sonar. The main disadvantage of multistatic sonar/sonobuoy systems is the increased system complexity and unusual sensing zones arising from the transmission losses (Karatas and Craparo 2015, Karatas et al, 2016; Craparo et al, 2017; Craparo et al, 2018, Craparo and Karatas 2018).

The probability of detecting a target with a monostatic sonobuoy depends mainly on the distance between the sonobuoy and the target. However, in a bistatic systems this probability is a function of both the source-target and target-receiver distances. In particular, the detection probability depends on the product of these two distances as shown in Figure 1. For a certain environmental condition, the sensing zone of a bistatic system is determined by its geometry and is characterized by Cassini ovals. Thus, the problem of devising optimal sensor configurations for bistatic sonobuoy systems is significantly more complex than the problem in monostatic systems. A key question is: what is the best deployment geometry of the sensors to successfully detect a submarine threat in a field of interest? Additionally, the analytical challenges with respect to the deployment of bistatic sonobuoys are exacerbated if the target of interest is not stationary.

This study is aimed at supporting ASW decision makers and planners in making the best use of bistatic sonobuoys during the search for stationary and mobile targets. In particular, we are interested in determining the optimal bistatic sonobuoy separation distance which maximizes the probability of detection *(PoD*) of (1) a target that is assumed to be stationary in the field of interest, and (2) a target that is assumed to be traversing the region of interest on a straight course. In addition to supporting practitioners who utilize bistatic sonobuoys, our results concerning this most fundamental multistatic system can serve as a foundation for future research efforts, including efforts to characterize and optimize other sensor systems.

We define two different scenarios involving mobile targets. In the first scenario, we consider a target that is initially located outside the field of interest enters the field and transits on a straight line (without any course changes). To determine the optimal sonobuoy deployment scheme (i.e., source-receiver separation distance), we first map the bistatic sonobuoy deployment problem to a line-set intersection problem. Next, using integral geometry and geometric probability we derive analytic expressions for the detection probability of the target. In scenario two, we consider a target which is initially located inside the region prior to sensor deployment. We assume that its initial location is determined uniformly at random, and that it moves on a straight line inside the region throughout the search period. To determine optimal sensor allocation schemes for this scenario, we model the region as a two-dimensional Poisson field of

targets as implemented in Washburn (2010) and Washburn and Karatas (2015). Next, we determine optimal source-receiver separation distances for different target speeds and search period lengths. We confirm the accuracy of our proposed solutions for both scenarios via Monte Carlo simulation.

Our primary goal is to demonstrate a method for using "back of the envelope" calculations to estimate bistatic sonar system performance. Although we do not address practical issues such as drifting of sonobuoys, tracking performance, energy management issues, multipath propagation, varying sensor and target depths, the deployment strategies proposed in this study can be used by designers to select key system parameters as well as to plan the geometry of the sonobuoys.

The organization of the paper is as follows. In Section 2, we provide a literature review pertaining to the deployment of bistatic and multistatic sonobuoy systems. Section 3 contains some preliminaries on bistatic sonobuoy detection criteria and the properties of Cassini ovals. In Section 4, we develop our analytic theory to determine optimal source-receiver separation distances of bistatic sonobuoy systems to detect stationary and mobile submerged targets. The comparison of analytical estimates with Monte Carlo simulation experiments appears in Section 5. We discuss various ways practitioners might apply our results in Section 6. Finally, Section 7 provides our conclusions and a discussion of possible extensions of our work.

2. RELATED WORK

A number of works in literature study the performance of bistatic and multistatic systems by using different techniques and approaches. Craparo et al (2017, 2018) and Craparo and Karatas (2018) review several papers which address multistatic sonar localization, scheduling, and performance measurement problems. Among these studies, Washburn (2010), Karatas et al (2014) and Washburn and Karatas (2015) consider a field of randomly deployed multistatic sensors and derive analytic formulas for approximating the coverage performance and cost effectiveness of the sonar network. Ozols and Fewell (2011) analyze the coverage performance of a number of multistatic sensor layouts with the objective of determining the most cost effective geometry. Similarly, using sonar equations, Fewell and Ozols (2011) develop a method to compute the detection performance of multistatic sonar network by comparing its performance to that of a similar network of monostatic sonars. In Wakayama et al (2011), the authors propose a methodology for forecasting the probability of target presence in an area of interest using tracking results from multistatic sonar devices.

Because of the analytical complexity associated with multistatic sonar systems, many researchers use heuristic methods to model detection probabilities and address sensor placement problems. For instance, Ngatchou et al (2006) use a particle swarm method to select the placement, number, and type of multistatic sonars to deploy, with the objective to maximizing area coverage. George and DelBalzo (2007) and Tharmarasa et al (2009) utilize a genetic algorithm to maximize area coverage and tracking performance of a multistatic sonar network. Similarly, Lei et al (2012) employ a genetic algorithm to determine optimal sensor placement for multistatic radar devices to detect moving targets.

A number of studies use simulation to analyze the performance of multistatic sonar networks. For example, Kalkuhl et al (2008) use a simulation-based methodology to plan multistatic search and rescue missions. Grimmett et al (2011) develop a sonar modeling and contact simulation tool that produces realistic simulated active sonar contact measurements in heterogeneous fields of mixed multistatic sonar sensors. They propose using the simulation output for information fusion and target tracking algorithms. Karatas and Craparo (2015) use simulation to evaluate the effect of direct blast zone to performance of multistatic sonar systems. Karatas et al (2016) use simulation to test the performance of multistatic networks which include a mobile source. Incze and Dasinger (2006) measure the performance of a multistatic network by

using an integrated Monte Carlo simulation and Bayesian technique. With the help of this combined methodology the authors aim to account for uncertainties such as target behavior and target probability distribution. In their study, Karatas and Akman (2015) determine the optimal bistatic sonobuoys sensor separation distance for stationary targets and they use simulation to verify their results. They find out that co-locating source and receiver is the best strategy to maximize the coverage of bistatic sonobuoys couple.

Coon (1997), Coraluppi (2006), Grimmett and Coraluppi (2004, 2006), Coraluppi and Carthel (2005), Coraluppi et al (2006), Hempel (2006), Gerard et al (2006), Erdinc et al (2006), Coraluppi et al (2007), Carthel et al (2007), Been et al (2007), Lang and Hayes (2007), Erdinc et al (2008), Ehlers et al (2009), Orlando et al (2010), Simakov (2008), Ozols et al (2011), Habtemariam et al (2011), Georgescu and Willett (2012), Grimmett and Wakayama (2013), Yang et al (2016), Peters (2017), Ristic et al (2017), Shi et al (2017) and Qin et al (2018) approach the bi/multistatic sensor location problem from the perspectives such as data fusion, target tracking and localization. Some of these studies aim to eliminate or reduce false alarms by converting multiple measurements collected by different sensors into a single track estimate. Krout et al (2006), Saksena and Wang (2008), Krout et al (2009) and Angley et al (2017) study the problem of multistatic sonar ping scheduling and they analyze ping schedules that maximize target detection probability and coverage. Among those studies, Saksena and Wang (2008) employ a Partially Observable Markov Decision Process (POM-DP) to develop efficient power management strategies for sonar devices. This improves system lifetime while maintaining acceptable detection performance. Krout et al (2009) develop a ping scheduling formulation based on sonar performance prediction and a Bayesian update utilizing target detection information. They show that by selecting intelligent ping sequences, it is possible to enhance the sonar system performance compared to random or sequential ping sequencing strategies. In more recent studies, Angley et al (2017a, 2017b) develop efficient ping scheduling methodologies for multistatic sonars that seek to improve tracking performance. Some other studies that consider the ping scheduling problem for bistatic and multistatic sonar include Wakayama and Grimmett (2010), Wakayama et al (2012), and Suvorova et al (2014).

In their study, Casbeer et al (2006) consider the connectivity issue for mobile multistatic radar networks which consist of unmanned air vehicles (UAVs). Strode (2011) also considers moving underwater targets and uses game theory to determine the positions of multistatic sonar devices to detect transiting underwater targets. The author also integrates his approach into a decision support tool called the Multistatic Tactical Planning Aid (MSTPA), developed at the Centre for Maritime Research and Experimentation (CMRE). Similarly, papers by Chen et al (2015), Gong et al (2016), and Wang et al (2016) consider mobile targets and approach the problem of developing efficient barriers against intruders by using bistatic radar. Walsh and Wettergren (2006) attempt to compute the detection probability of a mobile target moving on a straight line in a multistatic field of sources and receivers. The authors derive a model to approximate the detection probability of a target in terms of the location and orientation of its, track, the numbers of sources and receivers, and their location distribution functions. Wettergren (2008) considers the problem of detecting moving targets over large areas using a network of fixed sensor nodes and proposes the track-before-detect concept, which accounts for tracking information and multi-sensor data fusion. Lee et al (2017) propose a robust localization algorithm for bistatic sonar sensors that accounts for errors in the source position, receiver position, and sound speed. They use simulation to compare the performance of the algorithm with the conventional localization algorithms. Yang et al (2017) develop a closed form solution for localization of moving targets with multistatic sonars. The authors jointly use time delay, Doppler shift, and arrival angle measurement information, and they use simulation to confirm their results.

3. PRELIMINARIES

3.1 Bistatic Detection

In a bistatic sonar system detection occurs if the sound energy emitted by the source reflects off the target and generates an echo whose acoustic energy at the receiver exceeds the receiver's acoustic energy threshold. This threshold, *TH*, depends on the sensitivity of the receiver, environmental conditions and detection and false alarm settings. Based on the results in (Urick, 1983), for a bistatic system detection happens if

$$SL - TL_1 - TL_2 \geq TH \tag{1}$$

where *SL* is the source level and TL_1 and TL_2 are the transmission loss values from source to target and target to receiver, respectively, in decibels. If we further assume that the environment is homogeneous and the signal spreads in a spherical manner, the transmission loss between two points in the field follows a simple power law then for some constant $m > 0$, and we can rewrite Equation (1) as

$$SL - m\log(R_1) - m\log(R_2) \geq TH \tag{2}$$

where R_1 and R_2 denote the ranges from source to target and target to receiver respectively (Walsh and Wettergren, 2006). A common convention is to define the equivalent monostatic detection range $b = \sqrt{R_1 R_2}$, which is the geometric mean range of the system and represents the performance of a bistatic system when source and receiver are collocated (Willis, 2008; Washburn and Karatas, 2015). Solving Equation (2), we observe that detection occurs if

$$R_1 R_2 = b^2 \leq 10^{\frac{1}{m}(SL-TH)}. \tag{3}$$

Equation (3) is the well-known inequality that defines the interior of a Cassini oval as the detection region of a bistatic system (Cox, 1989). In this study, we use Equation (3) to model the detection region of a source-receiver couple, and we restrict our detection problem to two dimensions. Although we assume spherical spreading of the sonar signal, we also assume that the depth of potential targets is fixed and known. Thus, our sensor placement problem need only address detection at that depth. We now define some basic properties of Cassini ovals.

3.2 Cassini Ovals

Cassini ovals were first studied by Giovanni Domenico Cassini (1625–1712, aka Jean-Dominique Cassini) as a model for the orbit of the sun around the Earth (Ayoub, 1984). More recently, Cassini ovals have appeared in various scientific applications, including nuclear physics, acoustics, and the biosciences (Karatas, 2013). For example, researchers have used them in modeling human red blood cells (Mazeron and Muller, 1998; Di Biasio and Cametti, 2005), light scattering (Hellmers et al 2006), textile fabrics (Daukantiene et al 2003), population growth (Zong et al 2009), the evolutionary processes for morphogenetic sequences (Koenderink, 1990), the orbits of electrons (Beiser, 1997), and the cross-sectional area of a nuclear magnetic resonance coil (Allen et al 2002).

In James and James (1992), a Cassini oval is defined as "the locus of the vertex of a triangle when the product of the sides adjacent to the vertex is a constant and the length of the opposite side is fixed." Applying

this definition to the bistatic triangle in Figure 1, the vertex is at the target, b^2 denotes the constant, R_1 and R_2 are the sides adjacent to the vertex, and the separation distance, *2a*, between the source and receiver is the length of the opposite side.

If the sensors are fixed at $(\pm a, 0)$, the Cassini ovals are defined by:

$$\left((x-a)^2+y^2\right)\left((x+a)^2+y^2\right)=b^4, \qquad a,b\in\mathbb{R}. \tag{4}$$

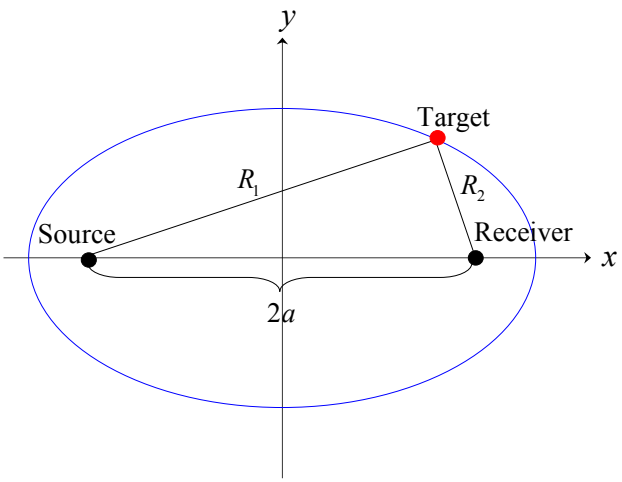

Figure 1. Bistatic triangle.

The curve is symmetric with respect to both axes, and its shape depends on the ratio of *a* to *b*. The ovals take on four qualitative forms:

- For $a/b \le \sqrt{2}/2$ the curve is a single loop that looks like an ellipse and intersects the *x* axis at $x=\pm\sqrt{a^2+b^2}$.
- For $\sqrt{2}/2 < a/b < 1$ the oval attains "dents" on its top and bottom.
- When $a/b=1$ the curve is a lemniscate of Bernoulli.
- For $a/b>1$ the curve splits into two ovals and there are two additional real *x* intercepts at $x=\pm\sqrt{a^2-b^2}$.

Figure 2 illustrates the ovals for different values of *a*/*b*, where *b* is fixed to 1 for simplicity.

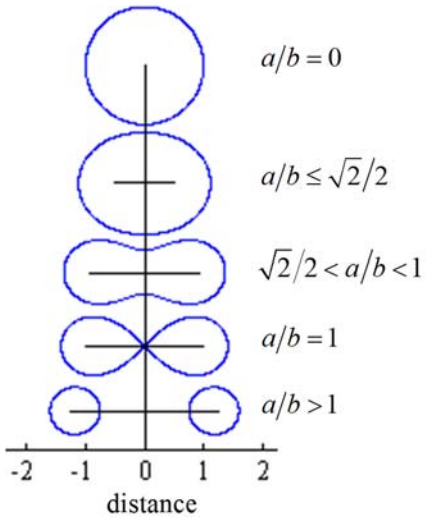

Figure 2. A family of Cassini ovals for b=1 (from Washburn and Karatas (2015)).

The area of a Cassini oval, denoted by A_C, can be calculated via a single numerical integration as follows. Since the oval is symmetric with respect to both axes we can compute A_C by multiplying the area of a quarter oval by four:

$$A_C = \begin{cases} 4\int_0^{\sqrt{a^2+b^2}} f_C(x)dx, & a/b \le 1 \\ 4\int_{\sqrt{a^2-b^2}}^{\sqrt{a^2+b^2}} f_C(x)dx, & a/b > 1 \end{cases} \tag{5}$$

where $f_C(x) = y = \pm\sqrt{-a^2 - x^2 \pm \sqrt{4x^2a^2 + b^4}}$ after solving (4) for y. To compute A_C one can also use the following approximation derived by (Willis, 2005):

$$A_C \approx \begin{cases} \pi b^2\left(1 - \frac{a^4}{4b^4} - \frac{3a^8}{64b^8}\right), & a/b \le 1 \\ \frac{\pi b^4}{2a^2}\left(1 + \frac{b^4}{8a^4} + \frac{3b^8}{64a^8} + \frac{25b^{12}}{1024a^{12}}\right), & a/b > 1. \end{cases} \tag{6}$$

Both the numerical integration (5) and the approximation (6) for A_C, normalized with respect to the monostatic area, πb^2, are plotted as a function of ratio a/b in Figure 3(*i*).

To compute the perimeter of a Cassini oval, denoted by P_C, we follow a similar approach by multiplying the arc length of a quarter oval by four. To do this, we use the infinitesimal calculus theorem which computes the arc length, S, of a function $f(x)$ between $x = x_l$ and $x = x_u$ by a single numerical integration (Weisstein, 2016) as:

$$S = \int_{x_l}^{x_u} \sqrt{1 + \left(f'(x)\right)^2}\, dx \tag{7}$$

where $f'(x)$ denotes the derivative of $f(x)$. Applying (7) to our case, P_C is computed as

$$P_C = \begin{cases} 4 \int_0^{\sqrt{a^2+b^2}} g_C(x)dx, & a/b \le 1 \\ 4 \int_{\sqrt{a^2-b^2}}^{\sqrt{a^2+b^2}} g_C(x)dx, & a/b > 1 \end{cases} \tag{8}$$

where

$$g_C(x) = \sqrt{1 + \left(f_C'(x)\right)^2} = \sqrt{\frac{b^4(a^2 - \sqrt{4x^2a^2 + b^4})}{(4x^2a^2 + b^4)(a^2 + x^2 - \sqrt{4x^2a^2 + b^4})}}. \tag{9}$$

Note that the area reaches its maximum value for a/b=0, whereas the perimeter is maximized when a/b=1. After the oval splits in two at a/b=1, the two parts continue shrinking in size as a/b increases, resulting in a steep decrease in perimeter (see Figure 3(*ii*)).

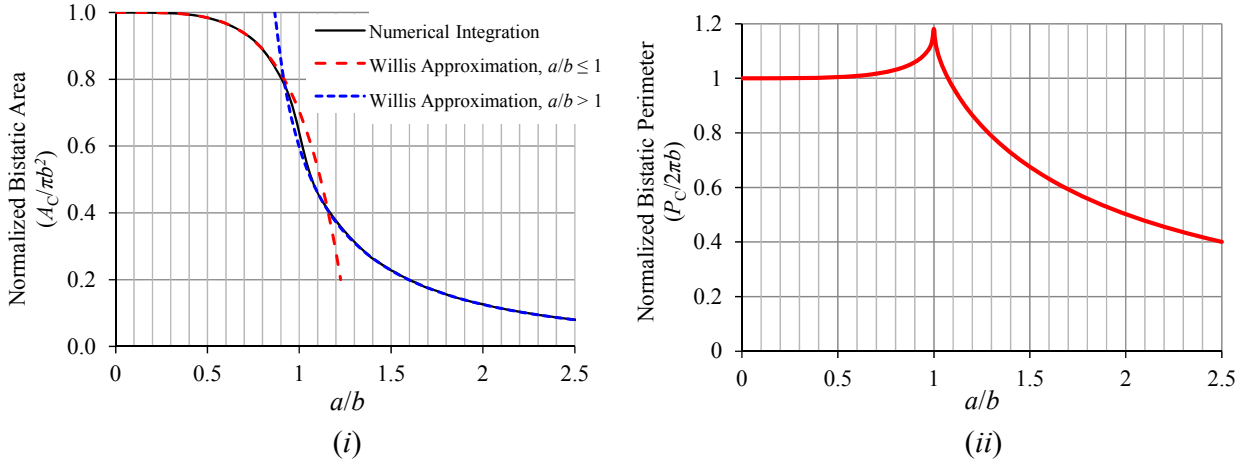

Figure 3. (i) Normalized bistatic area computed with numerical integration and Willis approximation. (ii) Normalized bistatic perimeter computed with numerical integration.

4. BISTATIC SONOBUOY DEPLOYMENT STRATEGIES

In this section we seek the optimal bistatic sonobuoy deployment strategies for stationary and moving targets under two scenarios. For both target types our goal is to determine the a/b ratio that maximizes the *PoD*. In general, a planner cannot control b (but knows its value), and can control a as well as the dimensionless ratio a/b.

4.1 General Assumptions

Assume that a bistatic sonobuoy couple with a monostatic detection range of $b > 0$ is deployed within the field of interest $F \subset \mathbb{R}^2$ where F is a connected and closed convex set with perimeter P_F and area A_F. The distance between the sensors (separation distance) is $2a \geq 0$. The bistatic couple can only detect events within its sensing zone $C \subset \mathbb{R}^2$ with perimeter P_C and area A_C, and a point in F is said to be covered if it is inside C (see Figure 4). Based on the geometric properties of Cassini ovals, when $a/b > 1$, C becomes two disjoint ovals denoted by C' and C'' with perimeters P'_C and P''_C. Let $conv(C)$ denote the convex hull of C when $a/b \leq 1$ and the convex hull of $C' \bigcup C''$ when $a/b > 1$, and denote the perimeter of $conv(C)$ by P_C^e. Following Santalo (1976), we define the *internal cover* of C' and C'' as the outline produced by a closed elastic string drawn about C' and C'' and crossing over at a point placed between C' and C'' as in Figure 4(*iii*). We denote the internal cover by C_i, with length P_C^i. For simplicity we assume that $A_F \gg A_C$.

We now discuss optimal bistatic sonobuoy deployments strategies for both stationary and mobile targets that move along straight lines.

4.2 Stationary Targets

First, we consider the problem of determining the optimal source-receiver separation distance to maximize the *PoD* of a stationary target. We assume that a stationary target is distributed uniformly at random over F. This assumption is reasonable for a scenario in which no prior information about the target location in the area exists. We wish to deploy a single bistatic source and receiver. We consider a definite range sensor model: if the target falls within the sensing zone C, it is detected with probability 1. Hence, the *PoD* of the target simply depends on the fraction of the area covered, i.e. $PoD = A_C / A_F$. Because A_F is fixed, maximizing A_C also maximizes the *PoD*.

Figure 3(*i*) reveals that the area A_C is maximized when $a/b = 0$, i.e., when the Cassini oval is a circle. This result implies that co-locating the source and receiver is the optimal strategy for detecting stationary targets. In other words, for the stationary target case with a single source and receiver, monostatic is better than bistatic. The interested reader can also refer to Karatas and Akman (2015) for a more comprehensive discussion of stationary target detection with bistatic sonobuoys.

4.3 Mobile Targets: Scenario 1

We now assume that a target transits F equiprobably. (The exact process by which the target's trajectory is generated appears in Section 5.2.) The target is detected with probability of 1 if T penetrates C, and otherwise it goes undetected. Lazos et al (2007) consider the problem of detecting mobile targets with monostatic sensors, where each sensor has an arbitrarily shaped sensing zone and all sensors are independent. They solve the problem by mapping it to a line-set intersection problem. We now use a similar approach.

4.3.1 Line-Set Intersection Problem:

We consider the following line-set intersection problem. Given a bounded set $K \subset \mathbb{R}^2$ with perimeter L, we wish to compute the probability that line ℓ intersects set $K_1 \subseteq K$ in each of three cases:

Case 1: K_1 is a convex set with perimeter L_1,

Case 2: K_1 is a non-convex (but simply connected) set with perimeter L_1, and

Case 3: K_1 is the union of two disjoint convex sets denoted by K_1' and K_1'' with perimeters L_1' and L_1'', respectively.

These cases are applicable to the bistatic detection problem when $a/b \le \sqrt{2}/2$ (Case 1), $\sqrt{2}/2 < a/b \le 1$ (Case 2), and $a/b > 1$ (Case 3). The field of interest *F* is represented by set *K*, while the target trajectory *T* is represented by line ℓ. Table 1 contains a complete mapping of the bistatic detection problem to a line-set intersection problem, and Figure 4 illustrates this mapping.

Table 1. Mapping the problem of detecting mobile targets with a bistatic sensor to a line-set intersection problem.

Mobile Target Bistatic Detection Problem	**Line Set Intersection Problem**
Field of interest *F* with perimeter P_F	Set *K* with perimeter *L*
Sensing zone *C* with perimeter P_C	Set K_1 with perimeter L_1
Sensing zones C' and C'' with perimeters P_C' and P_C''	Sets K_1' and K_1'' with perimeters L_1' and L_1''
Convex hull $conv(C)$ with perimeter P_C^e	Convex hull $conv(K_1)$ with perimeter L_1^e
Internal cover C_i with perimeter P_C^i	Internal cover K_1^i with perimeter L_1^i
Target trajectory *T*	Random line ℓ
PoD = Probability of detecting the target with 1. a convex sensing zone *C* 2. a single non-convex sensing zone *C* 3. at least one of the two disjoint convex sensing zones C' and C''	PoD_{K_1} = Probability of line ℓ intersecting 1. a convex set K_1 2. a non-convex, simply connected set K_1 3. at least one of two disjoint convex sets K_1' and K_1''

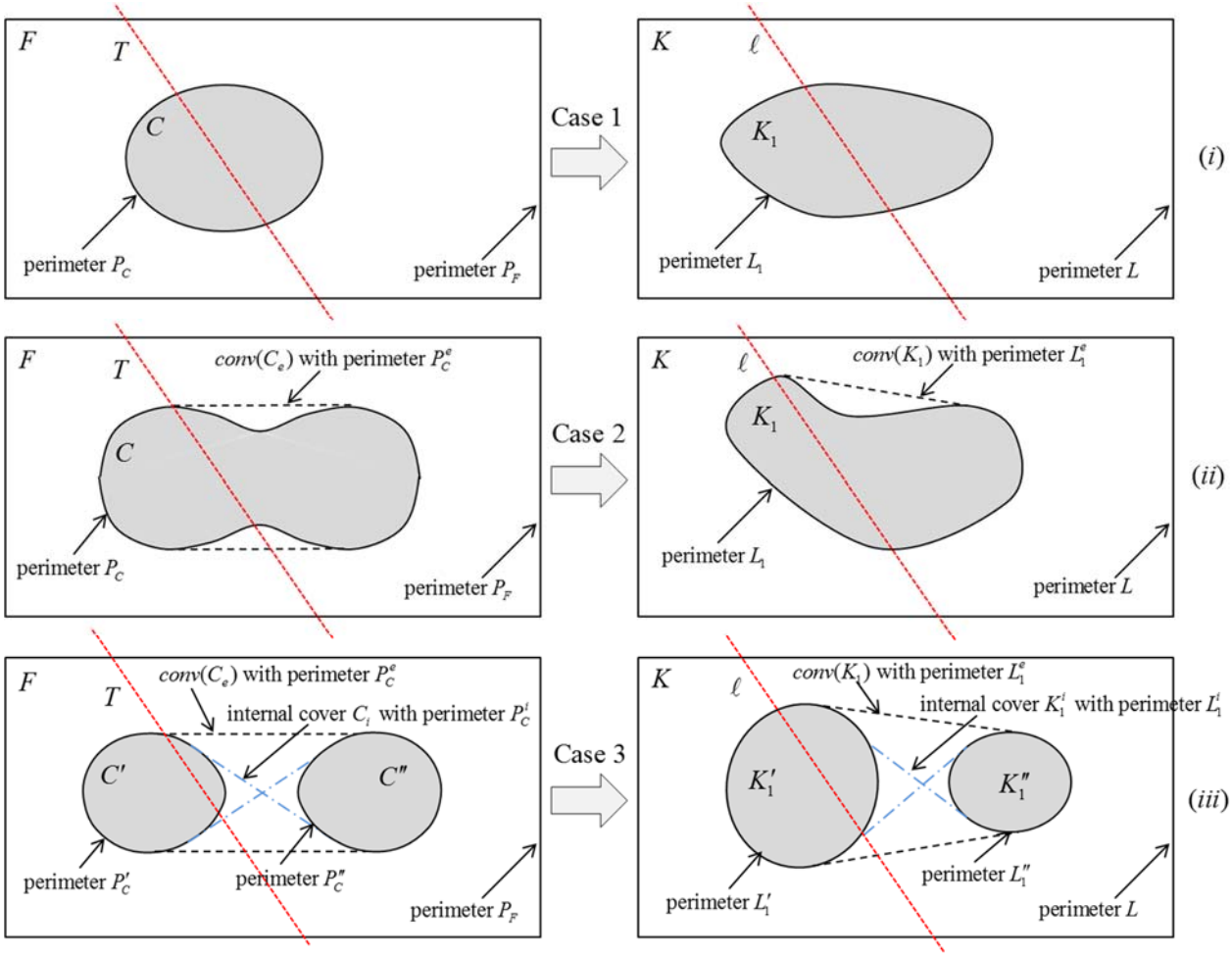

Figure 4. Mapping of the problem of detecting mobile targets with a bistatic sensor to a line-set intersection problem when the detection zone is (i) a convex set $(a/b \le \sqrt{2}/2)$ *(ii) a non-convex set* $(\sqrt{2}/2 < a/b \le 1)$ *(iii) two disjoint convex sets* $(a/b > 1)$.

4.3.2 Analytical Solution:

To solve the line-set intersection problem we adopt some results from integral geometry and geometric probability (Flanders, 1967; Lazos et al, 2007; Santalo, 1976). Proofs for Equations (11) and (12) and Theorems 1 and 2 can be found in (Santalo, 1976). For completeness, we include the proofs for Theorems 1 and 2 in the appendix.

A line ℓ can be specified by the shortest distance from ℓ to the origin of its coordinate system, ρ, and the angle of the direction perpendicular to ℓ with respect to the *x* axis, ϕ. The measure m of a set of lines $\ell(\rho,\phi)$ is defined by the integral of the density of lines $d\ell = d\rho \wedge d\phi$, where $\wedge$ denotes the exterior product used in exterior calculus (Flanders, 1967):

$$m(\ell) = \int d\rho \wedge d\phi. \tag{10}$$

The measure of set of lines that intersect a fixed bounded convex set *K* is

$$m(\ell;\ell \bigcap K \neq \varnothing) = \int_{\ell \bigcap K \neq \varnothing} d\rho \wedge d\phi = \int_0^{2\pi} \rho d\phi = L \tag{11}$$

where L is the perimeter of the set *K*.

Let *K* be a piecewise differentiable curve in the plane that has finite length *L*. The measure of all lines ℓ that intersect *K*, weighted by their number of intersections *n* times is given by

$$\int n d\ell = 2L. \tag{12}$$

Based on these definitions we now state two theorems from (Santalo, 1976).

Theorem 1 (Santalo, 1976)

If K_1 is a convex set with perimeter L_1 randomly deployed in a bounded set *K* with perimeter *L*, the probability that a random line ℓ intersecting *K* also intersects K_1, PoD_{K_1}, is given by:

$$PoD_{K_1} = \frac{L_1}{L}. \tag{13}$$

For the case where K_1 is non-convex, we must replace L_1 with the perimeter of $conv(K_1)$ (the convex hull of K_1), denoted by L_1^e. Similarly, if *L* is non-convex, *L* is switched with the perimeter of the convex hull of *K* (Santalo, 1976).

Returning to the multistatic sonar problem, for Case 1 where $a/b \leq \sqrt{2}/2$ (Cassini oval is a single loop that looks like an ellipse) we have

$$PoD = \frac{P_C}{P_F} \tag{14}$$

and for Case 2 where $\sqrt{2}/2 < a/b \leq 1$ (Cassini oval attains a dent on top and bottom) we have

$$PoD = \frac{P_C^e}{P_F}. \tag{15}$$

To address Case 3, we adopt Theorem 2 from (Santalo, 1976):

Theorem 2 (Santalo, 1976)

Let K_1' and K_1'' be two bounded convex sets in the plane such that $K_1' \bigcap K_1'' = \varnothing$, and denote their perimeters by L_1' and L_1'', respectively. Call $conv(K_1)$ the convex hull of $K_1' \bigcup K_1''$ and K_1^i the internal cover realized by a closed elastic string drawn about K_1' and K_1'' and crossing over at a point *O* placed between K_1' and K_1'' as in Figure 5. Let L_1^e and L_1^i denote the perimeters of $conv(K_1)$ and K_1^i,

respectively. Then, Santalo (1976) defines $PoS_{K',K''}$ as the probability that a random line ℓ separates K_1' and K_1'', given that it intersects $conv(K_1)$, and calculates it as follows:

$$PoS_{K',K''} = P(\ell \bigcap K_1' = \varnothing, \ell \bigcap K_1'' = \varnothing \mid \ell \bigcap conv(K_1) \neq \varnothing) = \frac{L_1^i - (L_1' + L_1'')}{L_1^e}. \tag{16}$$

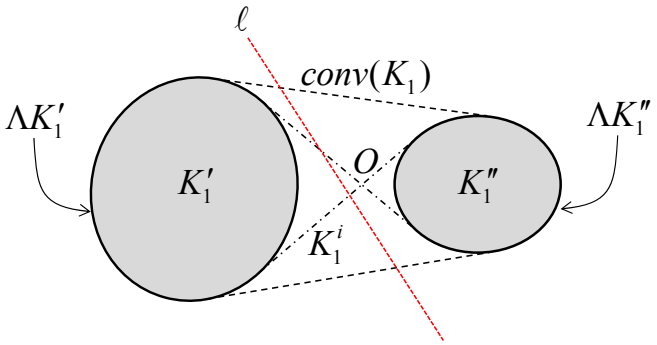

Figure 5. Two disjoint convex sets in a line-set intersection problem.

If we call $PoD_{K_1',K_1''}$ the probability that ℓ intersects either K_1' or K_1'' or both, given that it intersects $conv(K_1)$, then:

$$PoD_{K_1',K_1''} = 1 - PoS_{K_1',K_1''} = \frac{L_1^e - L_1^i + (L_1' + L_1'')}{L_1^e}. \tag{17}$$

Using (11) and (17), we can express $m_{K_1',K_1''}(\ell)$, the measure of set of lines that intersect either K_1' or K_1'' or both, as

$$m_{K_1',K_1''}(\ell) = L_1^e \cdot PoD_{K_1',K_1''} = L_1^e - L_1^i + (L_1' + L_1''). \tag{18}$$

Then,

$$PoD_{K_1} = \frac{m_{K_1',K_1''}(\ell)}{m(\ell; \ell \bigcap K \neq \varnothing)} = \frac{L_1^e - L_1^i + (L_1' + L_1'')}{L}. \tag{19}$$

Mapping (19) to our problem for Case 3 where $a/b > 1$ (Cassini oval splits into two ovals), we have

$$PoD = \frac{P_C^e - P_C^i + P_C}{P_F}. \tag{20}$$

To combine the mapping results in (14), (15), and (20), we define a new parameter, P_C^{eff}, as the effective perimeter of a Cassini oval as follows:

$$P_C^{eff} = \begin{cases} P_C, & a/b \le \sqrt{2}/2 \\ P_C^e, & \sqrt{2}/2 < a/b \le 1 \\ P_C^e - P_C^i + P_C, & a/b > 1 \end{cases} \tag{21}$$

and generalize *PoD* for all three cases as:

$$PoD = \frac{P_C^{eff}}{P_F}. \tag{22}$$

Given these results, we are now ready to calculate detection probabilities for sensing zones represented by Cassini ovals. In particular, we must compute P_C^e and P_C^i. Figure 6 shows a mathematical representation of a Cassini oval that will assist us in our calculations.

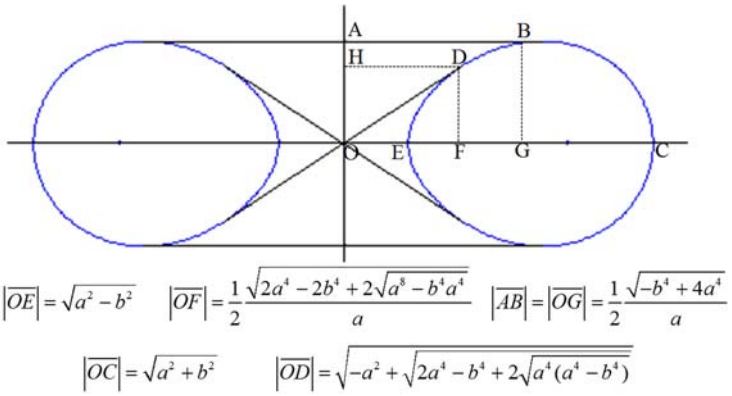

Figure 6. Geometrical representation of a Cassini oval and its intersection points on the x axis.

Similar to the P_C computation in (8), we use the symmetry property and multiply the length of a quarter of C_e and C_i by four. Using information in Figure 6 we can compute P_C^e and P_C^i as follows:

$$P_C^e = 4\left(\left|\overline{AB}\right| + \left|\widehat{BC}\right|\right) = 4\left(\frac{\sqrt{-b^4 + 4a^4}}{2a} + \int_{\frac{1}{2}\frac{\sqrt{-b^4+4a^4}}{a}}^{\sqrt{a^2+b^2}} g_C(x)dx\right) \tag{23}$$

$$P_C^i = 4\left(\left|\overline{OD}\right| + \left|\widehat{DC}\right|\right) = \left(\sqrt{-a^2 + \sqrt{2a^4 - b^4 + 2\sqrt{a^4(a^4 - b^4)}}} + \int_{\frac{1}{2}\frac{\sqrt{2a^4-2b^4+2\sqrt{a^8-b^4a^4}}}{a}}^{\sqrt{a^2+b^2}} g_C(x)dx\right). \tag{24}$$

Figure 7 represents P_C^{eff} normalized with respect to the monostatic perimeter, $2\pi b$, as a function of a/b ratio. It demonstrates that P_C^{eff} reaches its maximum value when a/b=1, meaning that to maximize *PoD* for transiting targets, we should separate the source and receiver by $2b$ thus gaining about 7% over a monostatic system where they are collocated.

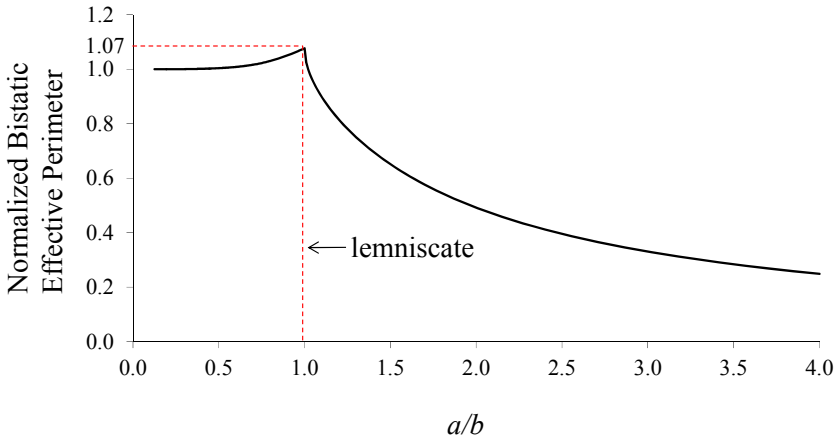

Figure 7. Normalized bistatic effective perimeter computed as $P_C^{eff}/2\pi b$.

4.4 Mobile Targets: Scenario 2

In this scenario we analyze the effect of target speed and search period on the optimal sensor configuration under the assumptions that the source and receiver are placed in a vast two-dimensional Poisson field of targets with density λ at time t=0 and the number of targets located in region F, N_F, follows a Poisson distribution of parameter $\lambda(A_F)$:

$$P(N_F = k) = \frac{e^{-\lambda(A_F)}\left(\lambda(A_F)\right)^k}{k!}. \tag{25}$$

We further assume that each target moves on a straight line through the field independently of other targets in a random direction $\theta \in [0, 2\pi)$ according to uniform distribution with a constant speed v for a finite period t. If the target enters C it is detected with probability 1. Given the initial target density and the random movement model, at any time instant t, the locations of the targets still form a two-dimensional Poisson field of the same density (Serfozo, 1999). If we call N_C the average total number of detections over t, we want to maximize $N_C = N_0 + N_t$ where N_0 is the average number of initial detections at time t=0 and N_t is the average number of detections in the time interval (0,t]. Initial detections include the targets that are inside the detection region C at time t=0, and based on the Poisson field assumption this is equal to $N_0 = \lambda A_C$.

N_t is computed by simply summing the number of targets that enter C up to time t. We approximate this by considering the sweeping of a Poisson field of stationary targets with a monostatic sensor of sweep width P_C^{eff}/π with a constant speed v for time t. In this approximation, the number of targets detected is computed as $N_t = \lambda \cdot \frac{P_C^{eff}}{\pi} \cdot v \cdot t$. Therefore,

$$N_C = \lambda\left(A_C + P_C^{eff} \cdot \frac{v \cdot t}{\pi}\right). \tag{26}$$

From (26) we note that the total number of detections depends on both A_C and P_C^{eff}. If we call A_{eq} the equivalent area covered and define it as the area in F that includes N_C targets, then $A_{eq} = N_C / \lambda$. Figure 8 illustrates the value A_{eq} with respect to vt and a/b. Note that, to maximize A_{eq}, one needs to adjust the separation distance of sonobuoys considering the product vt. The optimal a/b ratio for any given vt value is presented in Figure 9. In particular, the best strategy for $vt \le 5.77$ would be co-locating the sensors, or using an equivalent monostatic sensor with a detection range of b. For $5.77 < vt \le 17.8$ the optimal a/b value is between 0.82 and 1 (Cassini oval with dent on top and bottom), and for $vt > 17.8$ the optimal a/b value is 1 (lemniscate of Bernoulli).

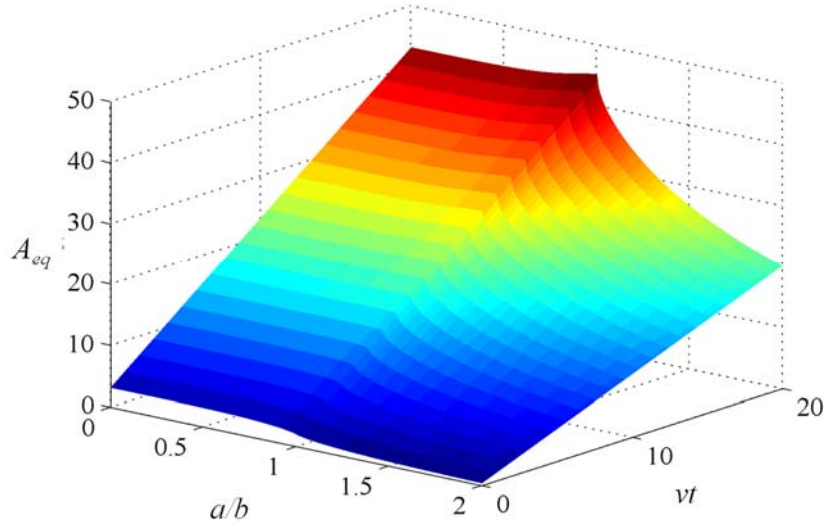

Figure 8. A_{eq} value (equivalent area covered by a stationary sensor) as a function of a/b and vt.

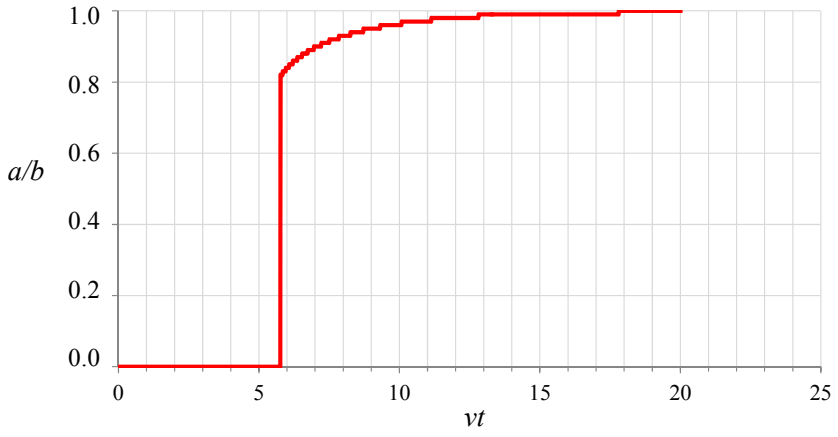

Figure 9. Optimal a/b value as a function of vt.

Comparing results from Karatas and Akman (2015) and Figures 7 and 8, we see that the stationary and moving target problems have different solutions. In practice all three tactical problems are important, with the emphasis depending on the target speed and the length of the time interval over which the buoys are

monitored. Although 0.5 is not the best *a/b* ratio in any case, it is a good compromise because it is nearly optimal in all cases.

5. SIMULATION RESULTS

In this section we perform Monte Carlo simulations to verify the theoretical results of detection probability for both stationary and moving targets. Without loss of generality we set b=1 in all simulation runs.

5.1 Experiments for Stationary Targets

Since there is no prior information about target location and the target is likely to be anywhere in the field, in our Monte Carlo simulations, we random uniformly place 10^6 targets in a rectangle of size 4x6 units.

Due to the fact that the source-receiver orientation does not have an effect on the area covered (A_C) at the beginning of our simulation for stationary targets, we place both the source and receiver at the center point of F. Then, at each iteration we increase the distance between source and receiver by 0.02 units as displayed in Figure 10(i). At each iteration we count the number of targets that lie within C.

Figure 10(i) illustrates a number of iterations of the simulation process. Solid lines represent bistatic detection zones (Cassini ovals) drawn for a series of different source-receiver locations. Targets are denoted by + marks. We repeat the experiment 10^3 times for difference target placements, and Figure 10(ii) shows the resulting average *PoD* values of the simulation results together with analytic function for all values of $a/b \in [0,2]$. Experiment results show an excellent match between the theory and simulation results. As predicted, *PoD* increases with A_C, and A_C attains its maximum value when *a/b*=0.

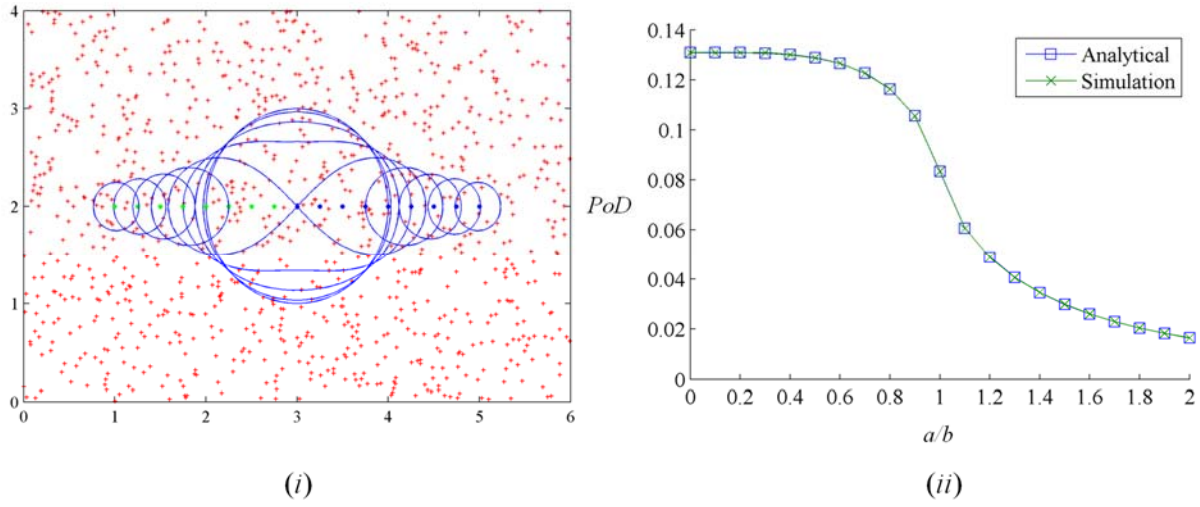

Figure 10. (i) Source and receiver locations for each iteration.
(ii) Comparison of simulation and analytic results with respect to different a/b ratios.

It should be noted that, although the ratio *a/b* = 0 is optimal, any *a/b* ratio between 0 and 0.5 leads to near-optimal results. Moreover, a strictly positive separation distance enables decision makers to take advantage of the covertness of multistatic systems, since the location of the receiver is unknown by the target.

5.2 Experiments for Mobile Targets: Scenario 1

To evaluate the detection performance of bistatic sensors for transiting targets we randomly deploy the bistatic couple with a fixed a/b value in a circular region F of radius r. We initially set the separation distance between buoys to 0 and increase it by 0.02 units until it reaches 4. To ensure statistical validity, for each a/b value we randomly deploy the buoys 10^3 times and for each deployment we generate 10^6 random mobile target trajectories as straight lines that intersect F as follows: Let F denote a circle of radius r with its center at the origin. We define a target trajectory by determining two points, the target entrance point (E_1) and exit point (E_2), on this circle. E_1 and E_2 are generated as follows:

1. Two angles, α_1 and α_2, are generated uniformly at random within $[0, 2\pi)$.
2. The coordinates of E_1 and E_2 are calculated as $\left(r\cos(\alpha_1), r\sin(\alpha_1)\right)$ and $\left(r\cos(\alpha_2), r\sin(\alpha_2)\right)$, respectively.
3. These two points are used to construct a target trajectory that enters F at point E_1, moves along a straight line, and exits F at E_2.

To compute PoD, for each a/b, we measure the fraction of trajectories that intersect with the sensing area of the sensors, C. Based on our results in previous section, the probability that a target is detected by a bistatic sonobuoy equals $PoD = P_C^{eff} / 2\pi r$. Figure 11(i) shows a simulation run. The disk of radius r represents the area F, while the Cassini oval represents the sensing zone C, and straight lines represent target trajectories. Figure 11(ii) depicts the detection probabilities for r=4 and 8 units and $a/b \in [0,2]$. The simulation results confirm that the probability of detecting a target travelling on a random straight line intersecting F is equal to the ratio of the perimeter of C (as computed by (21)) and the perimeter of F. Moreover, PoD is maximized when a/b=1.

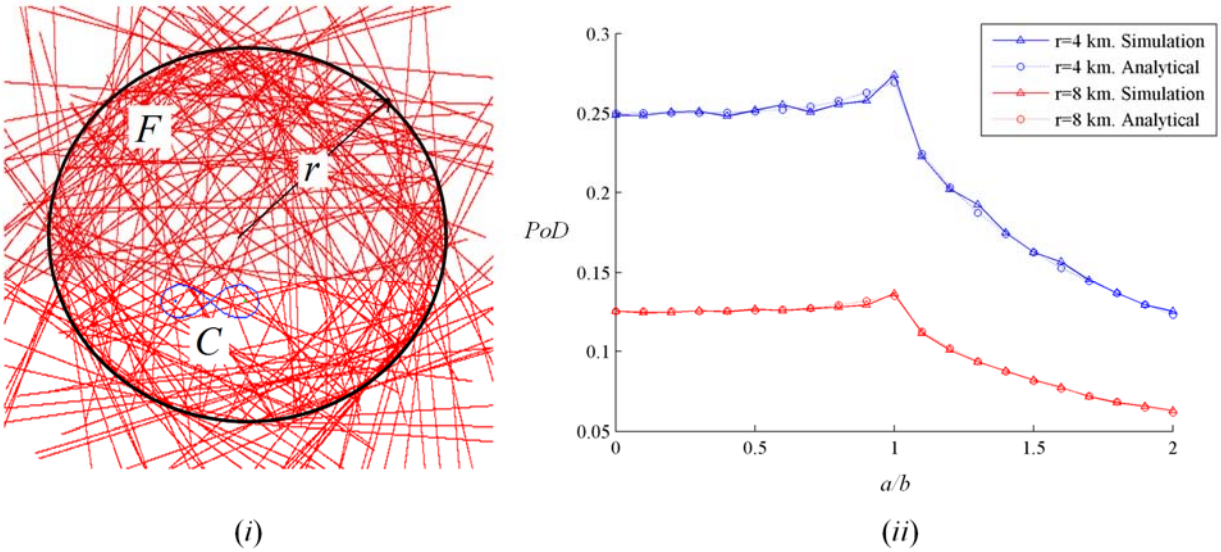

Figure 11. (i) A simulation run of transiting targets.
(ii) PoD values with respect to different a/b values for r=4 and 8 km.

5.3 Experiments for Mobile Targets: Scenario 2

In our final group of experiments for moving targets, we simulate a field F of size 50x50 units as a Poisson field of targets with density λ=2500 targets/unit^2. To simulate the vast Poisson field we choose the area size large enough to ensure that no target beyond the borders of F has a chance of entering C. We first place the sensors at the center of F and increase the distance from 0 to 4 units with increments of 0.02 units.

For each a/b value the targets move on a straight line in a random direction $\theta \in [0, 2\pi)$ according to uniform distribution. We measure the number of targets that are detected for two scenarios: one with vt=9 units and another with vt=20 units. Figure 12(i) displays an example simulation run. Figure 12(ii) displays both simulation and analytic results for vt=9 and 20 units and $a/b \in [0,2]$. The optimal a/b value is 0.95 for vt=9 units and 1.00 for vt=20 units.

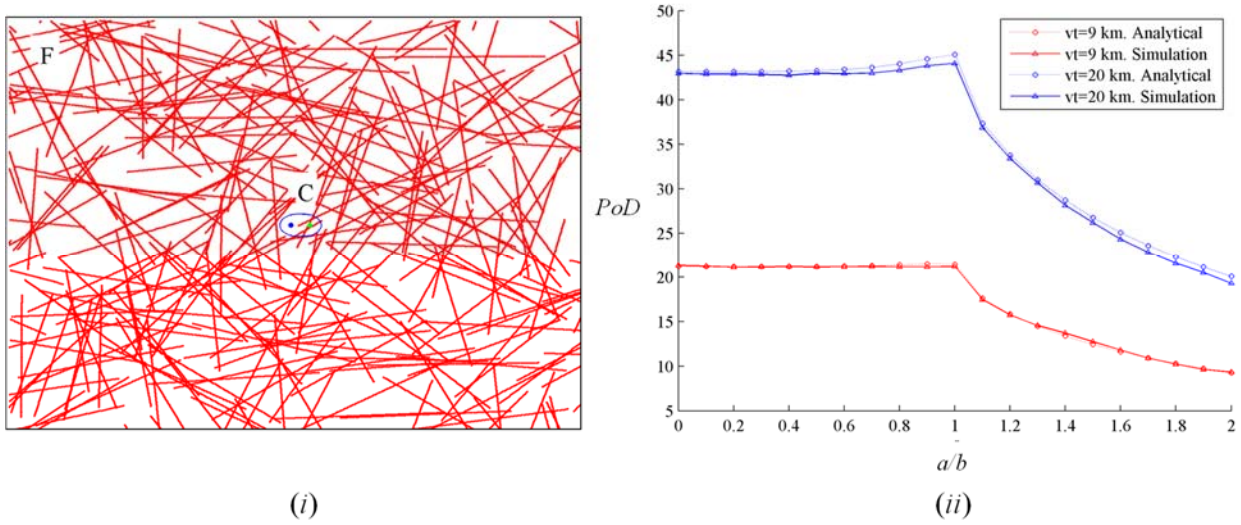

Figure 12. (i) Simulation run representing a Poisson field of targets moving in F. (ii) Analytical and simulation results of the number of detections for vt=9 and 20 units.

The simulation results confirm that the probability of detecting a random target travelling at a speed of v for a period of t in F depends on the magnitude of vt and the ratio a/b.

6. DISCUSSION

We now summarize our results and discuss their applicability to real-world decision problems. For the stationary target scenario, PoD simply depends on the fraction of the area covered and a/b=0 is the optimal value. For the moving target scenario where the target transits F on a straight line, we map the bistatic detection problem to a line set intersection problem and derive analytical expressions which result in an optimal ratio of a/b=1, thus a separation distance of $2b$. In the second and final moving target scenario where we assume that the sonobuoys are located in a Poisson field of targets where targets move to a random direction with a constant speed v for a finite period t, the optimal a/b value is determined to be between 0 and 1 depending on how large the vt product is. Even though all three problems have different solutions, a/b=0.5 provides an acceptable "compromise" solution since it is nearly optimal in all cases. Alternatively, a practitioner facing a target that is not known to be either stationary or moving could choose a/b in such a way as to provide some measure of robustness or to optimize an expected outcome. Let $PoD^{sta}(a/b)$ and $PoD^{mov}(a/b)$ denote the probability of detecting a stationary target and a moving target, respectively, as a function of the a/b ratio. Various approaches exist for selecting the a/b value that will provide the best balance between $PoD^{sta}(a/b)$ and $PoD^{mov}(a/b)$.

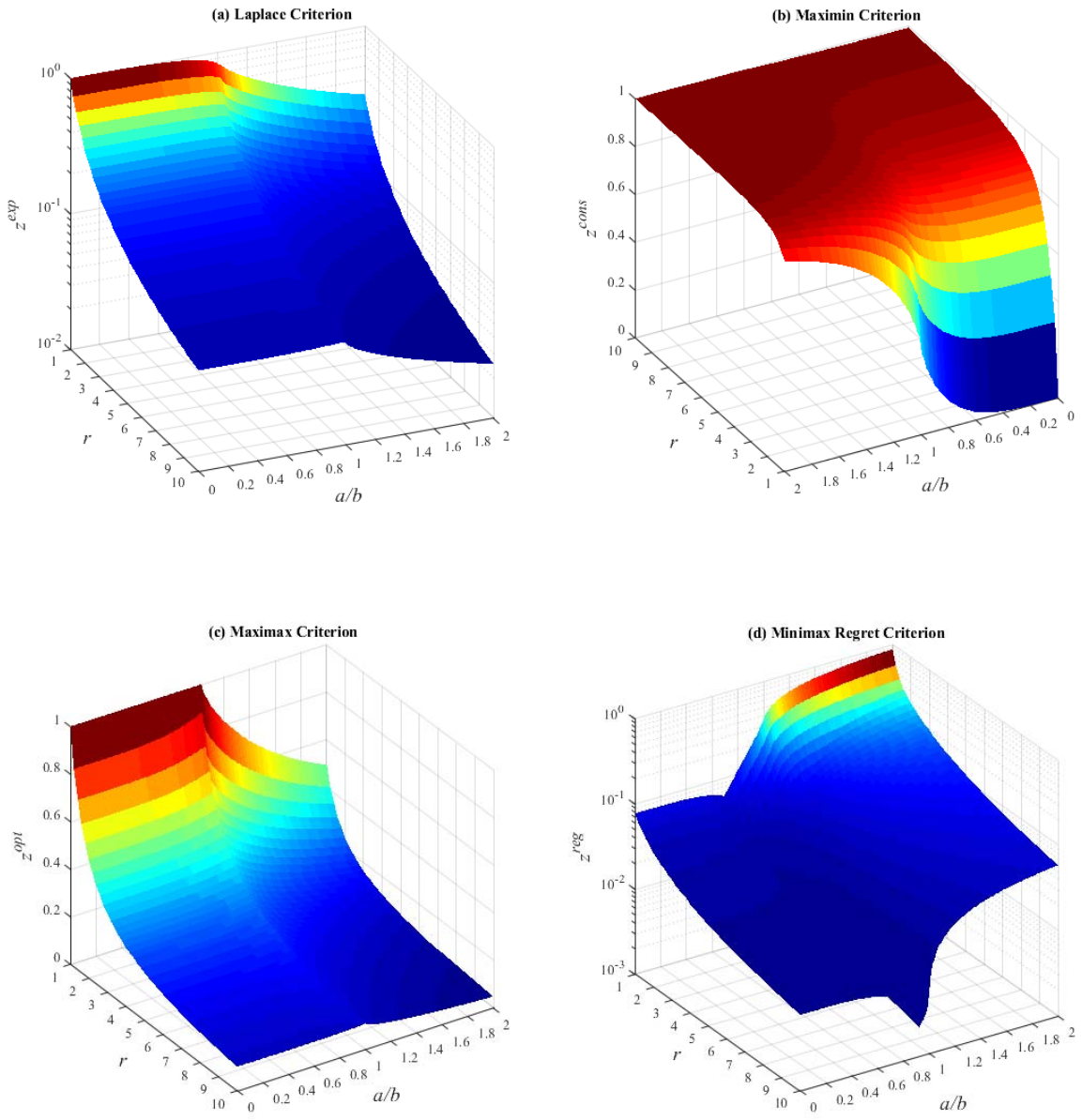

Figure 13. (a) z^{exp}, (b) z^{cons}, (c) z^{opt}, and (d) z^{reg} values for varying combinations of r and a/b. Note that the vertical axis in (a) and (d) uses a logarithmic scale. When using the Laplace, Maximin and Maximax criteria, a practitioner should choose the a/b ratio that maximizes z^{exp}, z^{cons} and z^{opt}, respectively. For the Maximin Regret criterion, it is optimal to choose the ratio that minimizes z^{reg}.

A natural choice is to choose the *a/b* ratio that maximizes the expected detection probability $z^{exp} = p^{sta} PoD^{sta}\left(a/b\right) + p^{mov} PoD^{mov}\left(a/b\right)$, where p^{sta} is the probability of encountering a stationary target, and p^{mov} is the probability of encountering a moving target. In the absence of reliable information regarding p^{sta} and p^{mov}, various options exist for choosing *a/b*. The Laplace criterion suggests setting $p^{sta} = p^{mov} = 0.5$ an maximizing z^{exp}. This approach assumes that if there is no information about the

probabilities on encountering a stationary or a moving target, then it is reasonable to treat the probability of encountering each type of target as being equal. Alternatively, the decision maker could use a conservative approach called the "Maximin criterion." This approach chooses *a/b* so as to maximize $z^{cons} = \min\{PoD^{sta}(a/b), PoD^{mov}(a/b)\}$. The Maximax criterion, on the other hand, is an optimistic approach that suggests examining the maximum payoff of each alternative and choosing the one with the best possible outcome. For our problem, this criterion maximizes $z^{opt} = \max\{PoD^{sta}(a/b), PoD^{mov}(a/b)\}$. Finally, the classical decision-theoretic notion of Minimax Regret suggests choosing *a/b* so as to minimize $z^{reg} = \max\{\max_{(a/b)^*}\left[PoD^{sta}\left((a/b)^*\right)\right] - PoD^{sta}(a/b), \max_{(a/b)^*}\left[PoD^{mov}\left((a/b)^*\right)\right] - PoD^{mov}(a/b)\}$.

Because both $PoD^{sta}(a/b)$ and $PoD^{mov}(a/b)$ depend on the radius of the search area, *r*, the resulting optimal also *a/b* ratio depends on *r*. Figure 13 shows the (a) z^{exp}, (b) z^{cons}, (c) z^{opt}, and (d) z^{reg} values for various combinations of *r* and *a/b*. In Figure 13(a), we use $p^{sta} = p^{mov} = 0.5$. Note that when using the Laplace, Maximin and Maximax criteria, a practitioner should choose the *a*/*b* ratio that maximizes z^{exp}, z^{cons} and z^{opt}, respectively. For the Maximin Regret criterion, it is optimal to choose the ratio that minimizes z^{reg}. Figure 14 shows the resulting optimal *a/b* for varying *r* values for all four criteria.

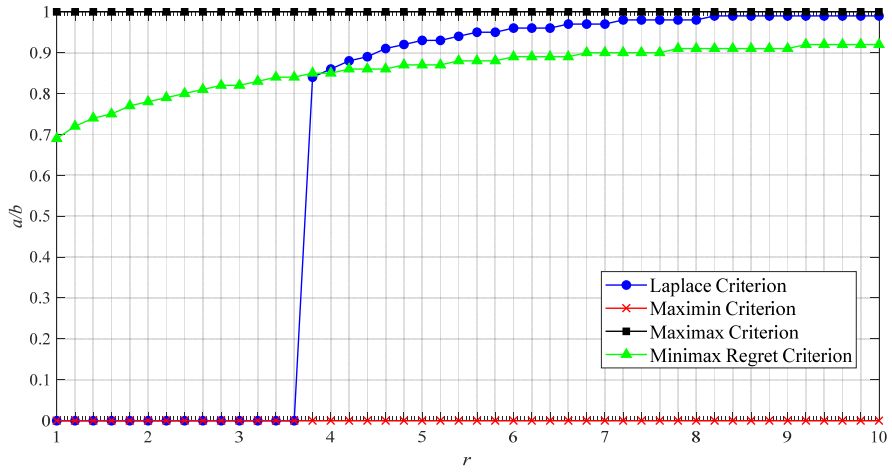

Figure 14. The best a/b ratio for various values of the search area radius r using Laplace, Maximin, Maximax and Maximin Regret criteria.

7. CONCLUSIONS AND FUTURE WORK

We have considered the problem of optimizing the placement of a bistatic sonobuoy pair for maximizing the target detection probability, *PoD*. Assuming that the geometric model of a bistatic system is a Cassini oval with a sensor separation distance of *2a* and equivalent monostatic detection range of *b*, the problem is to select the optimal *a*/*b* ratio so as to maximize *PoD* for both stationary and moving target scenarios. Our analysis provides a "back of the envelope" estimate of the probability of detection for each of these cases as a function of *a/b*. If it is not known whether the target is moving or stationary, the decision maker may choose an *a/b* value that provides some measure of robustness. The effectiveness and accuracy of our analytical solutions in this study are tested with Monte Carlo simulations, and our results show good agreement between the theory and simulation.

There are a variety of potential extensions of our work. We have made a number of simplifying assumptions in order to maintain analytical tractability, and these assumptions should be relaxed in future research efforts. Examples of additional elements that should be modeled include such phenomena as fluctuating signal strength (e.g., in the presence of noise or interference), the direct blast effect, alternative sensor models, target localization, Doppler shift, and target aspect dependence. Future work may also extend our approach to the multistatic setting, which is both important and non-trivial.

ACKNOWLEDGMENTS

Dr. Karatas was supported by the Scientific and Technological Research Council of Turkey (TUBITAK) (B.02.1.TBT.0.06.01-214-36-109). Dr. Craparo is funded by the Office of Naval Research (ONR). We gratefully acknowledge the anonymous reviewers of our manuscript, as well as Prof. Alan R. Washburn at Naval Postgraduate School, who contributed guidance and suggestions throughout this study.

Disclaimer*—The views and conclusions contained herein are those of the authors and should not be interpreted as necessarily representing the official policies or endorsements, either expressed or implied, of any affiliated organization or government.*

REFERENCES

Angley, D., Ristic, B., Suvorova, S., Moran, B., Fletcher, F., Gaetjens, H., & Simakov, S. (2017a). Non-myopic sensor scheduling for multistatic sonobuoy fields. IET Radar, Sonar & Navigation, 11(12), 1770-1775.

Angley, D., Suvorova, S., Ristic, B., Moran, W., Fletcher, F., Gaetjens, H., & Simakov, S. (2017b). Sensor scheduling for target tracking in large multistatic sonobuoy fields. In Acoustics, Speech and Signal Processing (ICASSP), 2017 IEEE International Conference on (pp. 3146-3150). IEEE.

Ayoub, R. (1984). "The lemniscate and Fagnano's contributions to elliptic integrals" Archive for history of Exact Sciences, 29(2), 131-149.

Allen P.S., Grove S., Zanche N. (2002). "Nuclear magnetic resonance birdcage coil with Cassinian oval former" United States Patent, US 6,452,393 B1.

Been, R., Jespers, S., Coraluppi, S., Carthel, C., Strode, C., & Vermeij, A. (2007). Multistatic sonar: a road to a maritime network enabled capability. Proceedings of Undersea Defence Technology Europe.

Beiser A. (1997). "Concept of modern physics" Tata McGraw Hill Publishing Company Ltd. N. Delhi. pp.131.

Carthel, C., Coraluppi, S., & Grignan, P. (2007, July). Multisensor tracking and fusion for maritime surveillance. In Information Fusion, 2007 10th International Conference on (pp. 1-6). IEEE.

Casbeer, D. W., Swindlehurst, A. L., & Beard, R. (2006). "Connectivity in a UAV multi-static radar network" American Institute of Aeronautics and Austronautics AIAA, 6209.

Chen, J., Wang, B., & Liu, W. (2015). "Constructing perimeter barrier coverage with bistatic radar sensors" Journal of Network and Computer Applications, 57, 129-141.

Cox, H., (1989), "Fundamentals of Bistatic Active Sonar", Underwater Acoustic Data Processing (Y. Chan, ed.), Kluwer, pp.3-24.

Coon, A. C. (1997). "Spatial correlation of detections for impulsive echo ranging sonar" Johns Hopkins APL Technical Digest, 18(1), 105–112.

Coraluppi, S. (2006). "Multistatic sonar localization" IEEE Journal of Oceanic Engineering, 31(4), 964-974.

Coraluppi, S., & Carthel, C. (2005). "Distributed tracking in multistatic sonar" IEEE Transactions on Aerospace and Electronic Systems, 41(3), 1138-1147.

Coraluppi, S., Carthel, C., & Hughes, D. (2007). Doppleraided multistatic sonar tracking. NURC Technical Report.

Coraluppi, S., Grimmett, D., & De Theije, P. (2006, July). “Benchmark evaluation of multistatic trackers” In Information Fusion, 2006 9th International Conference on (pp. 1-7). IEEE.
Craparo, E. M., & Karatas, M. (2018). “A Method for Placing Sources in Multistatic Sonar Networks” Technical Report NPS-OR-18-001 Naval Postgraduate School Monterey, CA.
Craparo, E., Karatas, M., Kuhn, T. (2017). “Sensor placement in active multistatic sonar networks” Naval Research Logistics, doi:10.1002/nav.21746.
Craparo, E., Fügenschuh, A., Hof, C., Karatas, M. (2018). “Optimizing source and receiver placement in multistatic sonar networks to monitor fixed targets” European Journal of Operational Research, ISSN 0377-2217, https://doi.org/10.1016/j.ejor.2018.02.006.
Daukantiene, V., Papreckiene, L., & Gutauskas, M. (2003). “Simulation and application of the behaviour of a textile fabric while pulling it through a round hole” Fibres and Textiles in Eastern Europe, 11(2), 37-41.
Di Biasio, A., & Cametti, C. (2005). “Effect of the shape of human erythrocytes on the evaluation of the passive electrical properties of the cell membrane” Bioelectrochemistry, 65(2), 163-169.
Ehlers, F., Daun, M., & Ulmke, M. (2009, May). “System design and fusion techniques for multistatic active sonar” In OCEANS 2009-EUROPE (pp. 1-10). IEEE.
Erdinc, O., Willett, P., & Coraluppi, S. (2006, July). Multistatic sensor placement: A tracking approach. In Information Fusion, 2006 9th International Conference on (pp. 1-8). IEEE.
Erdinc, O., Willett, P., & Coraluppi, S. (2008, June). The Gaussian mixture cardinalized PHD tracker on MSTWG and SEABAR’07 datasets. In Information Fusion, 2008 11th International Conference on (pp. 1-8). IEEE.
Fewell, M. P., & Ozols, S. (2011). “Simple Detection-Performance Analysis of Multistatic Sonar for Anti-Submarine Warfare” Technical Report DSTO-TR-2562 Defence Science and Technology Organisation Edinburgh, South Australia.
Flanders, H. (1967). “Differantial Forms”, Prentice Hall, NJ.
George, C., & DelBalzo, D. R. (2007). “Tactical planning with genetic algorithms for multi-static active sonobuoy systems” In 19th International Congress on Acoustics. Sociedad Espanola de Acustica (SEA).
Georgescu, R. & Willett, P. (2012). “The GM-CPHD Tracker applied to real and realistic multistatic sonar data sets” IEEE J. Ocean. Eng. 37, 220–235.
Gerard, O., Coraluppi, S., Carthel, C., & Grimmett, D. (2006, July). Benchmark analysis of NURC multistatic tracking capability. In Information Fusion, 2006 9th International Conference on (pp. 1-8). IEEE.
Gong, X., Zhang, J., Cochran, D., & Xing, K. (2016). “Optimal placement for barrier coverage in bistatic radar sensor networks” IEEE/ACM Transactions on Networking, 24(1), 259-271.
Grimmett, D., & Coraluppi, S. (2006, July). “Contact-level multistatic sonar data simulator for tracker performance assessment” In Information Fusion, 2006 9th International Conference on (pp. 1-7). IEEE.
Grimmett, D., & Coraluppi, S. (2004). “Sensitivity Analysis for Multistatic LFAS Localization Accuracy” Report SR-386 of the NATO Undersea Research Centre.
Grimmett, D., & Wakayama, C. (2013, July). Multistatic tracking for continous active sonar using Doppler-bearing measurements. In Information Fusion (FUSION), 2013 16th International Conference on (pp. 258-265). IEEE.
Grimmett, D., Wakayama, C., & Ricks, R. (2011, June). Simulation of passive and multistatic active sonar contacts. In Proceedings of the 4th International Conference on Underwater Acoustic Measurements: Technologies and Results.
Habtemariam, B. K., Tharmarasa, R., Kirubarajan, T., Grimmett, D., & Wakayama, C. (2011). Multiple detection probabilistic data association filter for multistatic target tracking. SPACE AND NAVAL WARFARE SYSTEMS COMMAND SAN DIEGO CA.
Hellmers, J., Eremina, E., & Wriedt, T. (2005). “Simulation of light scattering by biconcave Cassini ovals using the nullfield method with discrete sources” Journal of Optics A: Pure and Applied Optics, 8(1).

Hempel, C. G. (2006, September). “Adaptive track detection for multi-static active sonar systems” In OCEANS 2006 (pp. 1-6). IEEE.

James, G. and James, R. C. (1992). “Mathematics Dictionary”, 5th ed., D. Van Nostrand Co. Inc., New York, pp.47.

Incze, B. I., & Dasinger, S. B. (2006). “A Bayesian method for managing uncertainties relating to distributed multistatic sensor search” In 9th International Conference on Information Fusion (pp. 1-7). IEEE.

Kalkuhl, M., Wiechert, W., Nies, H., & Loffeld, O. (2008). “Simulation-based optimization of bi-and multistatic SAR missions” In 7th European Conference on Synthetic Aperture Radar (EUSAR) (pp. 1-4). VDE.

Karatas, M. (2013). “A Multi Foci Closed Curve: Cassini Oval, Its Properties and Applications” Dogus Universitesi Dergisi, 14 (2) 2013, 231-248 (2013).

Karatas M., and Akman G. (2015). “Bistatic sonobuoy deployment configuration for stationary targets,” Journal of Naval Science and Engineering, Vol.11, No.2, pp.1-10

Karatas M., Craparo, E. and Washburn, A.R. (2014). “A Cost Effectiveness Analysis of Randomly Placed Multistatic Sonobuoy Fields” The International Workshop on Applied Modeling and Simulation (WAMS 2014), Istanbul, Turkey, 16-17 September, 2014.

Karatas, M., Gunal M.M. and Craparo, E.M. (2016). “Performance Evaluation of Mobile Multistatic Search Operations via Simulation.” In Proceedings of the 2016 Spring Simulation Conference. IEEE Press. pp.110-115

Karatas, M., & Craparo, E. (2015). “Evaluating the direct blast effect in multistatic sonar networks using Monte Carlo simulation” In Proceedings of the 2015 Winter Simulation Conference (pp. 1184-1194). IEEE Press.

Koenderink J.J. (1990). “Solid shape (Artificial intelligence)” Massachusetts Institute of Technology, The MIT Press.

Krout, D. W., El-Sharkawi, M. A., Fox, W. L., & Hazen, M. U. (2006, July). Intelligent ping sequencing for multistatic sonar systems. In Information Fusion, 2006 9th International Conference on (pp. 1-6). IEEE.

Krout, D.W., Fox, W.L.J. and El-Sharkawi, M.A. (2009). “Probability of Target Presence for Multistatic Sonar Ping Sequencing”, IEEE Journal of Oceanic Engineering, Vol.34, No.4.

Lang, T., & Hayes, G. (2007, June). “Evaluation of an MHT-enabled tracker with simulated multistatic sonar data” In OCEANS 2007-Europe (pp. 1-6). IEEE.

Lazos, L., Poovendran, R. and Ritcey, J.A. (2007). “Probabilistic Detection of Mobile Targets in Heterogeneous Sensor Networks”, Proceedings of the 6th International Conference on Information Processing in Sensor Networks, pp.519-528.

Lee, K. H., Jeong, E. C., Kim, S., & Han, D. S. (2017). Robust localization using geographic information in bistatic sonar. International Journal of Distributed Sensor Networks, 13(6), 1550147717714172.

Lei, P., Huang, X., Wang, J., & Ma, X. (2012, July). Sensor placement of multistatic radar system by using genetic algorithm. In Geoscience and Remote Sensing Symposium (IGARSS), 2012 IEEE International (pp. 4782-4785). IEEE.

Mazeron, P., & Muller, S. (1998). “Dielectric or absorbing particles: EM surface fields and scattering” Journal of Optics, Vol 29, pp.68-77.

Ngatchou, P. N., Fox, W. L., El-Sharkawi, M. et al. (2006). “Multiobjective multistatic sonar sensor placement” In IEEE Congress on Evolutionary Computation (CEC) (pp. 2713-2719). IEEE.

Orlando, D., Ehlers, F., & Ricci, G. (2010). “A maximum likelihood tracker for multistatic sonars” In IEEE 13th Conference on Information Fusion, pp. 1-6.

Ozols, S., & Fewell, M. P. (2011). “On the Design of Multistatic Sonobuoy Fields for Area Search” Technical Report DSTO-TR-2563 Defence Science and Technology Organisation Edinburgh, South Australia.

Ozols, S., Fewell, M. P., & Thredgold, J. M. (2011). "Track-initiation probability for multistatic sonar fields" (No. DSTO-TN-1021). Technical Report DSTO-TR-2563 Defence Science and Technology Organisation Edinburgh, South Australia.

Peters, D. J. (2017). A bayesian method for localization by multistatic active sonar. IEEE Journal of Oceanic Engineering, 42(1), 135-142.

Qin, Z., Wei, S., & Wang, J. (2018). Efficient closed-form estimator for joint elliptic and hyperbolic localisation in multistatic system. Electronics Letters, 54(8), 525-527.

Ristic, B., Angley, D., Suvorova, S., Moran, B., Fletcher, F., Gaetjens, H., & Simakov, S. (2017). Gaussian mixture multitarget–multisensor Bernoulli tracker for multistatic sonobuoy fields. IET Radar, Sonar & Navigation, 11(12), 1790-1797.

Saksena, A., and Wang, I. J. (2008). "Dynamic Ping Optimization for Surveillance in Multistatic Sonar Buoy Networks with Energy Constraints" Proceedings of the 47th IEEE Conference on Decision and Control, 1109–1114.

Santalo, L. (1976). "Integral Geometry and Geometric Probability" 2nd ed., Addison-Wesley Publishing Company.

Serfozo, R. (1999). "Introduction to Stochastic Networks" Springer Verlag, New York, NY.

Shi, Y. F., Park, S. H., & Song, T. L. (2017). Multitarget tracking in cluttered environment for a multistatic passive radar system under the DAB/DVB network. EURASIP Journal on Advances in Signal Processing, 2017(1), 11.

Simakov, S. (2008). "Localization in airborne multistatic sonars" IEEE Journal of Oceanic Engineering, 33(3), pp. 278–288.

Strode, C. (2011). "Optimising multistatic sensor locations using path planning and game theory" In IEEE Symposium on Computational Intelligence for Security and Defense Applications (CISDA) (pp. 9-16). IEEE.

Suvorova, S., Morelande, M., Moran, B., Simakov, S., & Fletcher, F. (2014, July). Ping scheduling for multistatic sonar systems. In Information Fusion (FUSION), 2014 17th International Conference on (pp. 1-8). IEEE.

Tharmarasa, R., Kirubarajan, T., & Lang, T. (2009). "Joint path planning and sensor subset selection for multistatic sensor networks" In IEEE Symposium on Computational Intelligence for Security and Defense Applications (CISDA) (pp. 1-8). IEEE.

Urick, R. J. (1983). "Principles of Underwater Sound", 3rd ed., McGraw-Hill, New York, NY.

Wakayama, C. Y., & Grimmett, D. J. (2010, July). Adaptive ping control for track-holding in multistatic active sonar networks. In Information Fusion (FUSION), 2010 13th Conference on (pp. 1-8). IEEE.

Wakayama, C. Y., Grimmett, D. J., & Zabinsky, Z. B. (2011, July). Forecasting probability of target presence for ping control in multistatic sonar networks using detection and tracking models. In Information Fusion (FUSION), 2011 Proceedings of the 14th International Conference on (pp. 1-8). IEEE.

Wakayama, C. Y., Zabinsky, Z. B., & Grimmett, D. J. (2012). Linear optimization models with integer solutions for ping control problems in multistatic active acoustic networks. SPACE AND NAVAL WARFARE SYSTEMS CENTER PACIFIC SAN DIEGO CA.

Walsh, M.J. and Wettergren, T.A. (2006). "Search Performance Prediction for Multistatic Sensor Fields", Proceedings of OCEANS'08 MTS/IEEE Conference, Quebec City, QC.

Wang, B., Chen, J., Liu, W., & Yang, L. T. (2016). "Minimum cost placement of bistatic radar sensors for belt barrier coverage" IEEE Transactions on Computers, 65(2), 577-588.

Washburn, A. (2010). "A Multistatic Sonobuoy Theory", Naval Postgraduate School Technical Report, NPS-OR-10-005.

Washburn, A. and Karatas M. (2015). "Multistatic Search Theory", Military Operations Research (MOR) Journal, Volume 20/1, pp.21-38.

Weisstein, E.W. (2016). "Arc Length" From MathWorld -- A Wolfram Web Resource. http://mathworld.wolfram.com/ArcLength.html

Wettergren, T. A. (2008). Performance of search via track-before-detect for distributed sensor networks. IEEE Transactions on Aerospace and Electronic systems, 44(1).
Willis, N. J. (2008). “Bistatic Radar”, Radar Handbook, M. I. Skolnik (Editor in Chief), McGraw-Hill Professional, pp.23.4.
Willis, N. J. (2005). “Bistatic Radar”, 2nd ed., SciTech Publishing Inc., Raleigh, NC, pp.106.
Yang, L., Le, Y. and Ho, D. (2016). “Moving Target Localization in Multistatic Sonar by Differential Delays and Doppler Shifts” IEEE Signal Processing Letters, Issue 99.
Yang, L., Yang, L., & Ho, K. C. (2017, March). Moving target localization in multistatic sonar using time delays, Doppler shifts and arrival angles. In Acoustics, Speech and Signal Processing (ICASSP), 2017 IEEE International Conference on (pp. 3399-3403). IEEE.
Zong, Y., Yang, W., Ma, Q., & Xue, S. (2009). “Cassini growth of population between two metropolitan cities—A case study of Beijing-Tianjin region, China” Chinese Geographical Science, 19(3), 203-210.

APPENDIX

Proof of Theorem 1

Based on Equation (11), we can express this probability as the ratio of the measure of the set of lines intersecting K_1 to the measure of the set of lines intersecting K. For the case where K is convex:

$$PoD_{K_1} = \frac{m(\ell;\ell \bigcap K \bigcap K_1 \neq \varnothing)}{m(\ell;\ell \bigcap K \neq \varnothing)} = \frac{m(\ell;\ell \bigcap K_1 \neq \varnothing)}{m(\ell;\ell \bigcap K \neq \varnothing)} = \frac{L_1}{L} \tag{27}$$

If K_1 is non-convex and $conv(K_1)$ is the convex hull of K_1, one can observe that any line intersecting $conv(K_1)$ also intersects K_1, and vice versa. Thus, we have

$$PoD_{K_1} = \frac{m(\ell;\ell \bigcap K \bigcap conv(K_1) \neq \varnothing)}{m(\ell;\ell \bigcap K \neq \varnothing)} = \frac{L_1^e}{L}. \tag{28}$$

Therefore, in the case where K_1 is non-convex, L_1 is switched with the perimeter of $conv(K_1)$, L_1^e.■

Proof of Theorem 2

Let $\Lambda K_1'$ and $\Lambda K_1''$ be the boundaries of bounded convex sets K_1' and K_1'' respectively. Though they have arcs in common, we will consider $\Lambda K_1'$, $\Lambda K_1''$, $conv(K_1)$ and K_1^i as different curves. Every line that meets $\Lambda K_1'$ and $\Lambda K_1''$ has two intersection points with each of the curves $\Lambda K_1'$, $\Lambda K_1''$ and $conv(K_1)$, and four intersection points with K_1^i; there are in all ten points of intersection. Let m_{10} be the measure of the set of such lines. The lines that meet either $\Lambda K_1'$ or $\Lambda K_1''$, but not both, have six common points with the curves $\Lambda K_1'$, $\Lambda K_1''$, $conv(K_1)$, K_1^i and let m_6 be the measure of this set of lines. Similarly, the lines that separate $\Lambda K_1'$ and $\Lambda K_1''$ have four intersection points with the curves $conv(K_1)$ and K_1^i and let m_4 denote the measure of this set of lines.

Since the measure of the set of lines that meet a convex set is equal to its perimeter according to Equation (11), the measures m_6', m_6'' of the lines that meet K_1' without meeting and K_1'', or vice versa, are:

$$m_6' = L_1' - m_{10}, \qquad m_6'' = L_1'' - m_{10} \tag{29}$$

and therefore we have

$$m_6 = m_6' + m_6'' = L_1' + L_1'' - 2m_{10} \tag{30}$$

Since $conv(K_1)$ is a closed convex curve, we have

$$m_4 + m_6 + m_{10} = L_1^e \tag{31}$$

and applying (12) to sets $\Lambda K_1'$, $\Lambda K_1''$, $conv(K_1)$ and K_1^i, we obtain

$$4m_4 + 6m_6 + 10m_{10} = 2(L_1' + L_1'' + L_1^e + L_1^i) \tag{32}$$

and we get

$$\begin{aligned} m_4 &= L_1^i - (L_1' + L_1''), & m_6' &= L_1' - (L_1^i - L_1^e) \\ m_6'' &= L_1'' - (L_1^i - L_1^e), & m_{10} &= L_1^i - L_1^e \end{aligned} \tag{33}$$

In words, the measure of the set of lines that separate K_1' and K_1'' is $L_1^i - (L_1' + L_1'')$. In terms of geometrical probability, if ℓ is a line chosen at random in the plane with the condition that it meets the convex hull of K_1' and K_1'', the probability that ℓ separates K_1' and K_1'' is then $PoS_{K_1', K_1''} = P(\ell \bigcap K_1' = \varnothing, \ell \bigcap K_1'' = \varnothing, \ell \bigcap K_1^e \neq \varnothing) = \dfrac{L_1^i - (L_1' + L_1'')}{L_1^e}$.■